NANO LETTERS

Letter

pubs.acs.org/NanoLett

On-Chip Generation, Routing, and Detection of Resonance Fluorescence

G. Reithmaier,[†] M. Kaniber,*[,†] F. Flassig,[†] S. Lichtmannecker,[†] K. Müller,[†,§] A. Andrejew,[†] J. Vučković,[§] R. Gross,[‡,∥] and J. J. Finley*[,†,∥]

[†]Walter Schottky Institut und Physik Department, Technische Universität München, Am Coulombwall 4, 85748 Garching, Germany

[‡]Walther-Meißner-Institut, Bayerische Akademie der Wissenschaften und Physik-Department, Technische Universität München, 85748 Garching, Germany

[§]E. L. Ginzton Laboratory, Stanford University, Stanford, California 94305, United States

[∥]Nanosystems Initiative Munich (NIM), Schellingstraße 4, 80799 München, Germany

Supporting Information

ABSTRACT: Quantum optical circuits can be used to generate, manipulate, and exploit nonclassical states of light to push semiconductor based photonic information technologies to the quantum limit. Here, we report the on-chip generation of quantum light from individual, resonantly excited self-assembled InGaAs quantum dots, efficient routing over length scales ≥1 mm via GaAs ridge waveguides, and in situ detection using evanescently coupled integrated NbN superconducting single photon detectors fabricated on the same chip. By temporally filtering the time-resolved luminescence signal stemming from single quantum dots we use the quantum optical circuit to perform time-resolved excitation spectroscopy on single dots and demonstrate resonance fluorescence with a line-width of 10 ± 1 μeV; key elements needed for the use of single photons in prototypical quantum photonic circuits.

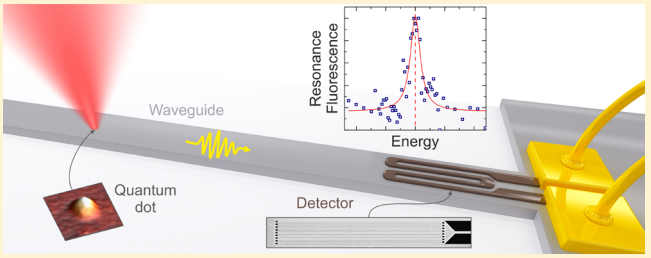

KEYWORDS: *Integrated quantum optics, nano photonics, superconducting single photon detectors, quantum dots, resonance fluorescence*

Nonclassical light can be generated by resonant excitation of individual quantum emitters to scatter single photons with coherence properties determined primarily by the excitation laser source.[1] By carefully tailoring the local optical mode density experienced by the emitter, coherent and incoherent nonclassical light can be preferentially routed into low loss waveguide modes and distributed on a chip into a quantum photonic circuit.[2−5] In recent years strong quantum light−matter couplings in such photonic nanostructures have been shown to produce effective interactions between photons leading to remarkable phenomena such as photon blockade,[6−8] needed for optical transistors,[9,10] photonic quantum gates,[11,12] and ultrafast optical switching with only a few control photons.[13] While the generation and routing of quantum light on a semiconductor chip has already been demonstrated by several groups,[14−16] the ability to generate and route single photons on-chip and detect them *in situ* with near unity quantum efficiency[17] would represent a major step toward the realization of semiconductor based quantum optical circuits. Hereby, superconducting single photon detectors (SSPDs) are particularly useful due to their very high detection efficiencies,[18−21] low dark count rates,[22] sensitivity from the visible to the IR,[23] and picosecond timing resolution.[24,25] Single photon detection in such devices arises from the formation of a normal conducting hotspot in the thin superconducting nanowire.[26] Since the bias current is slightly subcritical (typically ∼0.95I_{crit}), the local heating arising from single photon absorption results in the breakup of Cooper pairs, local switching of the nanowire to a normal conducting state, thus giving rise to a measurable voltage pulse in the external readout circuit. The possibility to integrate SSPDs onto dielectric[27,28] and plasmonic[29−31] waveguides facilitates evanescent coupling to waveguide photons, pushing the single-photon detection efficiency toward unity. Both the generation of cluster states of photonic qubits for one-way quantum computation[32] and the measurement based teleportation schemes[33] rely on having such a near perfect detection efficiency.

As depicted schematically in Figure 1a the samples investigated consist of a linear GaAs (core)−AlGaAs/air (cladding) multimodal ridge waveguide into which a single layer of optically active self-assembled InGaAs quantum dots (QDs) is embedded at its midpoint, 125 ± 5 nm below the surface. A single-frequency tunable diode laser (line-width < 1 MHz, modulated at ∼3 GHz to produce 290 ± 70 ps pulses at a

Received: April 14, 2015
Revised: June 18, 2015

DOI: 10.1021/acs.nanolett.5b01444
Nano Lett. XXXX, XXX, XXX−XXX

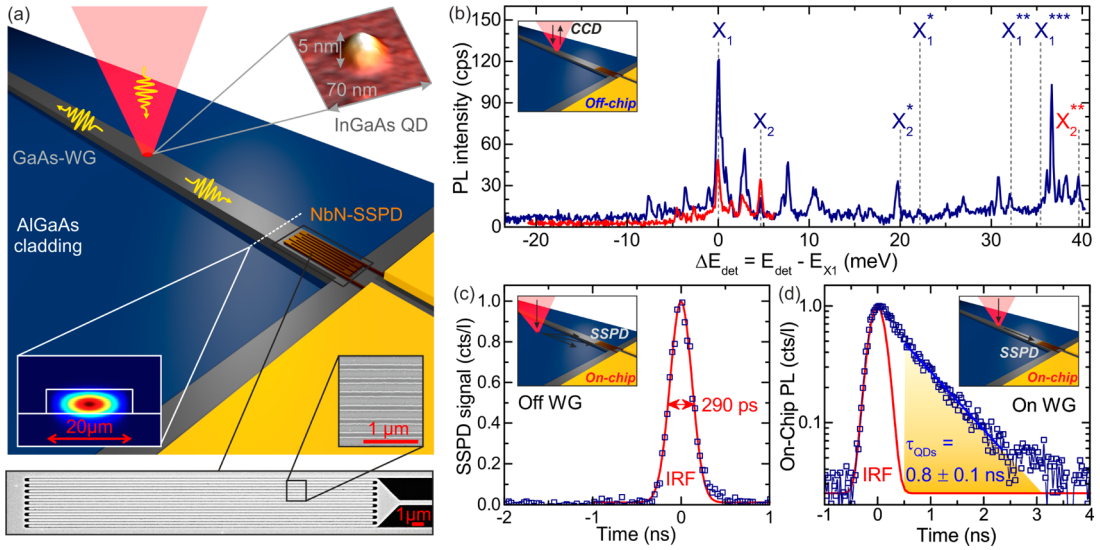

Figure 1. (a) Sample structure combining a 2 mm long GaAs ridge waveguide (FDTD simulation of the fundamental mode profile as an inset) containing a single layer of InGaAs QDs, as shown in the AFM image on the top right, which are evanescently coupled to an NbN-SSPD. An SEM image of the SSPD is shown on the lower panel. (b) PL intensity detected in confocal geometry for excitation in the wetting layer at 1347.7 meV (blue curve) and at X_2^{**} (red curve). In the text we focus on the two quantum dot transitions labeled X_1 and X_2. The corresponding excited state transitions that we study are labeled $X_{1,2}^{*}$, $X_{1,2}^{**}$, and X_1^{***}, respectively. (c) Instrument response function (IRF) of the electrically modulated excitation laser, detected on-chip using the SSPD. The signal is plotted in units of counts per detected laser photon (cts/l). (d) Typical time transient of multiple quantum dots excited in the wetting layer and detected on-chip using the integrated SSPD. The IRF is shown in red, whereas the integration window used to extract the intensity originating solely from the QD emission is indicated by the yellow shaded region.

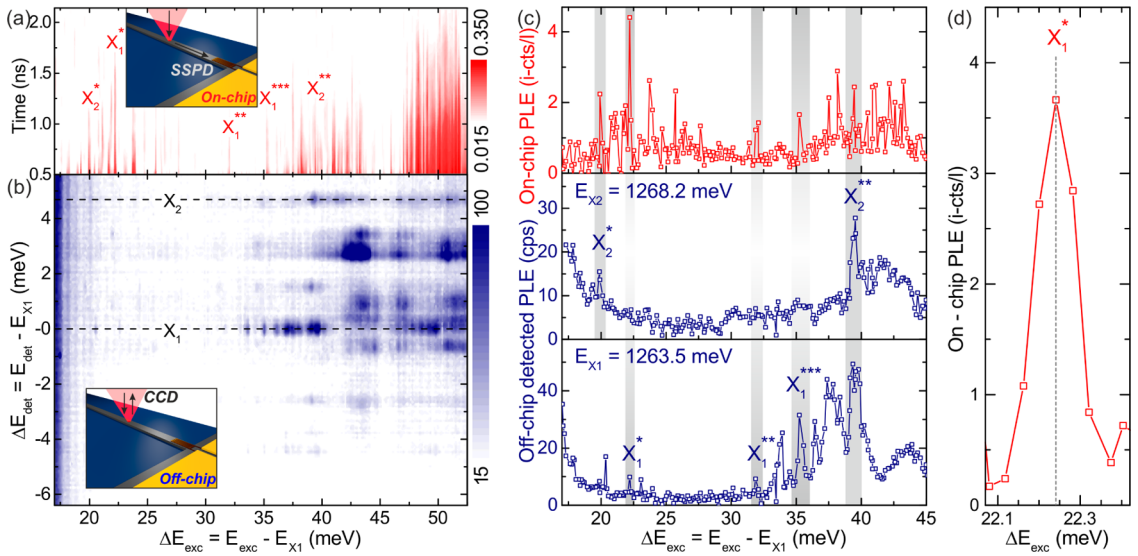

Figure 2. (a) Time-resolved on-chip PL intensity as a function of energy difference ΔE_{exc} between the laser E_{exc} and the X_1 transition E_{X_1}. The lines that we focus on are marked $X_{1,2}^{*}$, $X_{1,2}^{**}$, and X_1^{***}. (b) Spectrally filtered, off-chip detected PL intensity for the same range of excitation energy as probed in the on-chip measurement. The two highlighted lines X_1 and X_2 correspond to the QD transitions presented in Figure 1b. (c) Top panel: Integrated on-chip PL intensity for times >0.5 ns plotted as a function of ΔE_{exc}. The on-chip signal is plotted in units of integrated counts per detected laser photon (i-cts/l). Middle/bottom panel: PL intensity detected in off-chip geometry along the two lines marked in (b). The five common resonances that we focus on are highlighted by the gray shaded regions and labeled with respect to the spectrum shown in Figure 1b. (d) High-resolution scan with on-chip detection of resonance X_1^{*}.

3% duty cycle) is focused onto the waveguide surface, producing a diffraction limited spot with ~3−5 self-assembled QDs within the focal volume (Figure 1a). The light generated and scattered by the excited QDs is then guided along the ridge waveguide over a distance $\Delta x = 1040 \pm 1$ μm and evanescently coupled into the nanowires of an integrated SSPD as shown in the scanning electron microscopy image in Figure 1a. By varying Δx while recording the QD photoluminescence (PL) using the integrated SSPD[34] we determined the propagation losses to be 6.6 ± 0.5 dB/mm. A simulated photonic mode profile for a $w_{WG} = 20$ μm wide waveguide is shown as an inset of Figure 1a, demonstrating the strong confinement of light in the waveguide; this gives rise to near-unity absorption of waveguide-photons in the active detection region.[35] Therefore, this simplistic quantum optical circuit provides a test bed for

DOI: 10.1021/acs.nanolett.5b01444
Nano Lett. XXXX, XXX, XXX−XXX

all-optical generation, distribution, and detection of nonclassical light on the photonic chip.

First, we performed off-chip detected confocal PL measurements for various positions along the waveguide in order to identify regions with only a few sharp emission lines originating from individual dots. Typically, the emission intensity recorded from the QDs near the edge of the waveguide can be more readily measured in this off-chip geometry since a larger fraction of the total emission emerges from the sample surface. This can clearly be seen in the spatially resolved luminescence images presented on similar samples.[38] Although the waveguide coupling efficiency for such dots is limited, they provide the potential to determine their spectral emission characteristics in off-chip PL measurement. Therefore, we focus intentionally on dots close to the periphery of the waveguide to facilitate on- and off-chip measurements of the same quantum emitter. Typical results of such off-chip detected confocal PL measurements are presented in Figure 1b that compare emission spectra recorded from one such position with the laser frequency tuned into the wetting layer at E_{WL} = 1347.7 meV (blue curve) and quasi-resonant excitation via an excited QD resonance, labeled X_2^{**} in Figure 1b, at $E_{X_2^{**}}$ = 1302.8 meV (red curve). For this excitation position and both excitation energies we observe pronounced emission from the same line labeled X_1 in Figure 1b at E_{X_1} = 1263.5 meV and weaker emission from the line labeled X_2 at E_{X_2} = 1268.2 meV. As shown in the Supporting Information (section S2), the intensity of both emission lines increases linearly with the excitation power (P) according to $I \propto P^m$ with exponents of m = 0.96 ± 0.02 and 0.99 ± 0.04, respectively, identifying both features as arising from single exciton transitions.[36] We will continue to probe the absorption properties of X_1 and X_2 using PL−excitation (PLE) spectroscopy later in Figure 2a,b with both on-chip detection via the integrated SSPD and off-chip detection via an imaging monochromator (see methods). The bottom axis of Figure 1b shows the energy difference $\Delta E_{det} \equiv E_{det} - E_{X_1}$ between the detection energy (E_{det}) and the X_1 ground state emission energy. Whereas the emission lines X_1 and X_2 are attributed to ground state transitions of two different QDs, the lines $X_{1/2}^{*}$, $X_{1/2}^{**}$, and X_1^{***} marked in Figure 1b are identified as arising from excited QD states, an attribution supported by the PLE measurements discussed below.

Performing on-chip PLE spectroscopy using the integrated SSPD is complicated by the fact that it is sensitive to *all* light propagating within the waveguide mode (i.e., no spectral filtering). Moreover, the SSPD detects any background signal originating from laser stray light scattered at the back surface of the sample as well as laser light that is directly coupled into the waveguide. In an effort to reduce the impact of scattered laser light we polished the back surface of the sample and sputtered an amorphous silicon absorber layer to reduce the index contrast and, thereby, the impact of scattering. Furthermore, this layer also absorbs the scattered excitation laser light (see methods). In addition, we utilized pulsed laser excitation in combination with temporal filtering of the SSPD signal to separate the directly scattered laser light from the QD luminescence. Figure 1c shows a typical example of the time-resolved SSPD signal following excitation next to the waveguide where all QDs have been completely removed by etching. In this case, only scattered laser light reaches the SSPD, and the time-resolved SSPD signal reveals a Gaussian instrument response function (IRF). The temporal resolution of ±70 ps given throughout this Letter reflects the resolution of the high-frequency detection electronics since the SSPD response is much faster (~70 ps).[35] In strong contrast, upon exciting the waveguide region containing QDs via the underlying wetting layer we observe an exponentially decaying SSPD signal that can clearly be seen in Figure 1d. The deconvolution of the observed SSPD signal with the IRF reveals a clear monoexponential decay with a lifetime of τ_{QDs} = 0.80 ± 0.07 ns, typical for the InGaAs QDs in this sample.[36] In order to completely separate the QD signal from the laser stray light, the detected time-resolved SSPD signal was temporally integrated for times ≥0.5 ns onward, as illustrated by the yellow shaded region in Figure 1d.

This technique to distinguish the on-chip QD-PL signal from scattered laser light reaching the SSPD facilitates the investigation of the PLE response of the X_1 transition. Thereby, the excess laser energy $\Delta E_{exc} \equiv E_{exc} - E_{X_1}$ was tuned over a range of 17.0 meV ≤ ΔE ≤ 52.5 meV in steps of 0.1 meV. The corresponding time-resolved transients for on-chip detection and the ΔE-dependent off-chip multichannel PLE data showing the X_1 and X_2 peaks are presented in Figure 2a,b, respectively. For large excess excitation energies ΔE_{exc} = 47.5 → 52.5 meV, a strong on-chip signal is observed with closely spaced sharp lines in PLE, which we attribute to WL 0D−2D bound-continuum transitions[37] (see Figure 2a,b). Moving to more resonant excitation energies (ΔE_{exc} = 46.0 ± 1.0 meV), we simultaneously observe a suppression of luminescence in both on- and off-chip measurements. This observation reflects the absence of continuum transitions[37] for more resonant excitation. For excess laser energies in the range ΔE_{exc} ≤ 44.0 meV the PLE spectrum exhibits several discrete absorption resonances on a weak background (see Figure 2a,b). The three resonances labeled X_1^{**}, X_2^{**}, and X_1^{***} in Figure 2a will be focused on later in the discussion related to Figure 2c. Most interestingly, we observe a group of long time-transients labeled $X_{1/2}^{*}$ for ΔE_{exc} < 25.0 meV in Figure 2a and corresponding weak QD emission features as shown in Figure 2b. These states are tentatively attributed to p-shell transitions of the QD emission lines X_1 and X_2, consistent with the expected orbital quantization energy $\Delta E_{s-p} \approx$ 20 meV for such InGaAs QDs.[38] This identification is further supported by the fact that no additional PLE resonances are observed in the on-chip data for ΔE_{exc} < 17.5 meV down to the s-shell transition. We note that the increasing background observed in the off-chip measurement for ΔE_{exc} < 17.5 meV (Figure 2b,c bottom panels) arises from scattered laser light at the sample.

We continue by focusing on the energy range between 20.0 meV < ΔE_{exc} < 45.0 meV, where several pronounced and clearly separated excited state resonances for both on- and off-chip detection geometries are observed. The lower two panels of Figure 2c show the off-chip PLE spectra detecting at the energies of X_1 and X_2, respectively, whereas the upper panel shows the time integrated on-chip SSPD signal for $t \geq$ 0.5 ns to exclude the scattered laser light. When comparing the on- and off-chip PLE measurements presented in Figure 2c, several common features can be identified as highlighted by the gray shaded regions. For example, at ΔE_{exc} = 20.0 meV a clear resonance is observed in the on-chip signal shown in the upper panel of Figure 2c, while simultaneously a clear resonance is observed in the PLE spectrum detecting on X_2 (Figure 2c middle panel). In total, we focus on two distinct PLE resonances (X_2^{*}, X_2^{**}) for X_2 and on the three resonances

DOI: 10.1021/acs.nanolett.5b01444
Nano Lett. XXXX, XXX, XXX−XXX

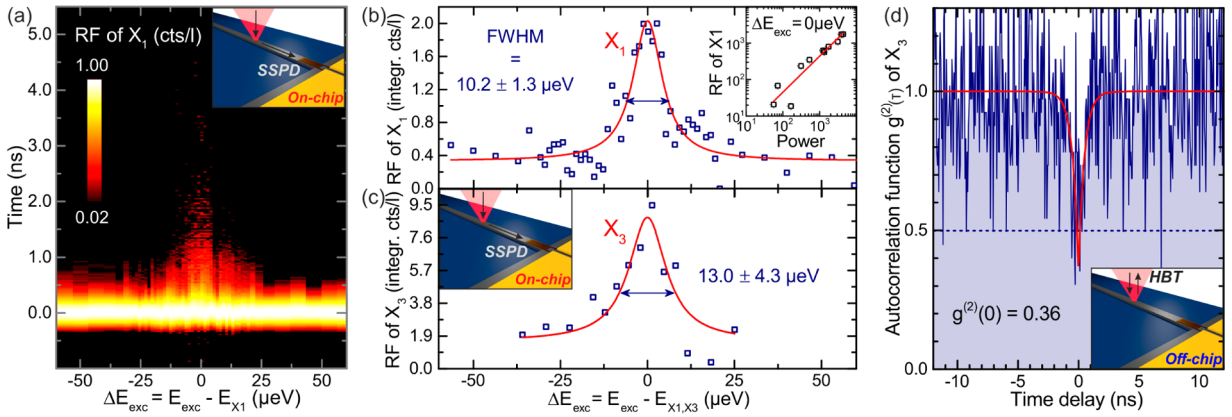

Figure 3. (a) Time-resolved resonance fluorescence signal obtained from X_1, as detected in on-chip geometry using the integrated SSPD. The data is color coded in counts per detected laser photon (cts/l). (b,c) Integrated RF signal of X_1 and X_3 for a time-window from 0.5 to 5.0 ns (blue squares) showing a Lorentzian line-shape (red solid line) with a fwhm of 10.2 ± 1.3 and 13.0 ± 4.3 μeV, respectively. Inset in (b): Linear power dependence of the RF signal for 0 μeV laser detuning. (d) Autocorrelation function $g^{(2)}(\tau)$ measured for QD transition X_3 with an emission energy of $E(X_3)$ = 1296 meV under quasi-resonant continuous wave excitation at 1362 meV shown in blue. The deconvoluted fit to the data is shown in red, resulting in $g^{(2)}(0) = 0.36$.

X_1^*, X_1^{**}, and X_1^{***} for X_1 and marked them in Figure 2c. A high-resolution scan with on-chip detection of X_1^* is presented in Figure 2d, showing a Lorentzian shaped resonance at ΔE_{exc} = 22.24 meV. In addition to the highlighted resonances, a number of weaker features were detected in the confocal PL data between 23.0 meV < ΔE_{exc} < 30.0 meV and found to be correlated with resonances observed in the on-chip PLE in the same energy interval. In summary, common QD resonances are observed both in off- and on-chip PLE measurements, indicating that the integrated SSPD has sufficient sensitivity to discriminate emission from an individual quantum emitter.

After demonstrating that our on-chip integrated SSPDs are capable of measuring on-chip PLE, while simultaneously collecting off-chip PLE of QD excited state resonances, we continue to demonstrate resonance fluorescence (RF) from the s-shell transition X_1. Hereby, we fine-tuned the excitation laser in steps of δE = 1 μeV across X_1 and simultaneously recorded on-chip time-resolved transients for each laser excitation energy. As discussed in the Supporting Information (section S3), resonance fluorescence in such patterned photonic systems typically requires the use of a second, weak nonresonant laser tuned above the bandgap of the GaAs waveguide (E = 1.534 eV, P = 0.06 ± 0.02 W/cm^2) to continuously create free carriers in the vicinity of the QD under study and, thereby, stabilize the fluctuating electrostatic environment.[39,40] In Figure 3a, we present time-resolved transients recorded as a function of detuning $\Delta E_{exc} = E_{exc} - E_{X_1}$ while scanning the laser across the s-shell resonance X_1. We clearly observe resonantly excited QD time transients over an energy range ΔE_{exc} = ±20 μeV with respect to the QD exciton ground state energy E_{X_1}. The observed signal exponentially decays with a lifetime of 0.70 ± 0.07 ns, clearly showing that it arises from QD emission. The on-chip recorded RF signal, integrated over a temporal range of 0.5−5 ns, is presented in Figure 3b as a function of excitation energy ΔE_{exc} = ±60 μeV, exhibiting a pronounced peak at ΔE_{exc} = 0 μeV. Fitting the data with a Lorentzian line shape ($2A/\pi \times \Delta_{fwhm}/(4\Delta E_{exc}^2 + \Delta_{fwhm}^2)$, with the peak area A) we extracted a line width of Δ_{fwhm} = 10.2 ± 1.3 μeV, in excellent agreement with values recently reported for off-chip detected RF from QDs embedded in a free-standing single-mode ridge waveguide.[40] The inset of Figure 3b shows the power dependence of the temporally integrated RF signal detected at ΔE_{exc} = 0 μeV as a function of the excitation laser power. The observed linear dependence is expected for the 290 ± 70 ps pulses used since the excitation pulse duration exceeds the QD coherence time of $T_2 = \hbar/\Delta E$ = 65 ± 8 ps, and thereby, coherent Rabi dynamics are expected to be weak. Similar resonance fluorescence measurements were made on several different dots within the waveguide with similar results to those presented in Figure 3a,b. Figure 3c shows one example RF spectrum from another dot labeled X_3 emitting at 1296.6 meV (PL spectra presented in the Supporting Information section S2). Using a Lorentzian fit (red solid line) we extract the line width of X_3 to be 13.0 ± 4.3 μeV, identical to the RF signal obtained from X_1 within experimental accuracy. In order to demonstrate the quantum nature of the on-chip detected light we performed off-chip measurements of the photon statistics of X_3. Since emission is predominantly into the WG mode, the signal recorded in off-chip detection is weak. However, this particular QD emission line exhibits a very clean ground state emission signal S with little background B, resulting in an emission coefficient[41] of $\delta = S/(S + B)$ = 0.92 ± 0.05. When filtering X_3 using a monochromator and sending it into a Hanbury−Brown and Twiss setup, we measured the autocorrelation function $g^{(2)}(\tau)$, as presented in Figure 3d. Here, the background corrected[41] coincidence counts detected from the QD emission are plotted as a function of time delay, whereas the red solid line shows a deconvoluted fit to the data. From the fit we extract a $g^{(2)}$-value at zero delay time of <0.5 ($g^{(2)}(0) = 0.36 \pm 0.07$), thus indicating the quantum nature of the emitted quantum dot luminescence. The observation of antibunched emission from X_3, which exhibits a clear RF signature in our on-chip measurements, provides strong evidence that the on-chip RF signal observed in our experiments represents nonclassical light in the prototype quantum optical circuit shown in Figure 1a.

In summary, we presented the creation, routing, and detection of quantum light on a single chip. By temporally filtering the on-chip detected, time-resolved luminescence signal, we suppress the background generated by the excitation laser, demonstrating that specific QD excited state resonances can be observed in both on- and off-chip detection geometries. Applying this time-filtering technique, we demonstrated

DOI: 10.1021/acs.nanolett.5b01444
Nano Lett. XXXX, XXX, XXX−XXX

resonance fluorescence from a single QD with a line-width of 10.2 ± 1.3 μeV, guided in the optical modes of a GaAs ridge waveguide and efficiently detected via evanescent coupling to an integrated NbN-SSPD on the same chip. By measuring the autocorrelation function of similar QDs using off-chip detection and simultaneously showing on-chip detected resonance fluorescence, we prove the nonclassical character of the detected light. The results of this prototype quantum optical circuit provide a test bed for all-optical generation, distribution, and detection of nonclassical light on a common photonic chip.

Methods. *Sample Preparation.* The samples investigated were grown using solid source molecular beam epitaxy and consisted of a 350 μm thick GaAs wafer onto which a 2 μm thick $Al_{0.8}Ga_{0.2}As$ waveguide cladding layer was deposited. Following this, a 250 nm thick GaAs waveguide core was grown into which a layer of self-assembled InGaAs QDs was embedded at its midpoint. The growth conditions used resulted in dots with a typical lateral (vertical) size of 25 ± 5 nm (5 ± 1 nm) as shown in the top-right inset of Figure 1a, an areal density of 6 ± 1 μm^{-2} and PL emission around ∼ 1348 meV at 4 K with an inhomogeneously broadened ensemble line width of 83 meV. After growth, the native oxide was removed from the sample surface using an HCl dip, and a high quality 10 ± 0.5 nm thick NbN superconducting film was deposited using DC reactive magnetron sputtering. By carefully optimizing the deposition temperature, rate, and Nb/N ratio, high quality superconducting films were obtained on the GaAs substrate (T_C = 11.9 ± 0.2 K), despite the 26% lattice mismatch.[42,43] To suppress the scattering of laser stray light into the detector, the backside of the sample was chemically and mechanically polished using a 5% Br_2/Ch_3OH solution, and an absorbing Si layer was grown on the backside of the sample using electron beam evaporation. As described in detail in the Supporting Information section S6, scattered laser light on the SSPD is only an issue for excitation energies below the GaAs bandgap for which the substrate is transparent. For such below gap excitation scenarios, the signal-to-background ratio (η) reduces significantly from $\eta \geq 420$ for above gap excitation, to $\eta \leq 3$ for sub-bandgap excitation. To circumvent this effect, the polishing of the sample backside was employed to reduce the RMS roughness to <20 nm decreasing the diffuse light scattering by 1 order of magnitude. Moreover, we coated the backside of the wafer with a 1 μm thick amorphous Si-layer to reduce the index contrast at the rear surface and efficiently absorb photons with $E_{exc} \geq 1.2$ eV at the back side of the sample (for details see Supporting Information section S6). While these combined measures increased η by more than 2 orders of magnitude, the obtained values remained too high for on-chip detection of QD luminescence via the SSPD. To further suppress the direct detector illumination by laser stray light originating from the top, a sequence consisting of 50 ± 15 μm Teflon, 12 ± 0.5 μm aluminum foil, and 50 μm Teflon foil was carefully placed over the detector under an optical microscope. The complete sandwich structure (shown in the Supporting Information section S5) was then fixed to the side of the chip carrier.

The nanowire detectors were then defined using electron beam lithography with a negative tone resist and reactive ion etching using a SF_6/C_4F_8 plasma to form two NbN nanowire meanders, each consisting of 18x, 100 ± 5 nm wide nanowires separated by 150 ± 5 nm to form two detectors, each with a width of 4.5 μm and a total length of 30 μm along the waveguide axis. Of those two detectors, only one has been employed to measure the data presented in this Letter. A scanning electron microscope image of one resulting NbN detector on GaAs is presented in Figure 1a inset at the bottom. Subsequently ∼2600 μm long, 20 μm wide multimodal ridge waveguides were defined using photolithography and wet etching in a citric acid + H_2O_2 solution. The waveguides were defined such that a pair of nanowire detectors is centered on one end, penetrating ∼60 μm into the waveguide end to ensure optimum evanescent coupling.[14] For future use, single mode waveguides will be advantageous over multimodal waveguides. However, as a test bed for such an integrated device, multimodal waveguides are easier to fabricate and puts less stringent requirements on the relative position of the waveguide with respect to the SSPDs. Furthermore, the used multimodal waveguides with a width of 20 μm also give rise to a sufficiently high number of potential quantum dots coupling to the propagating mode.

Device Operation and Characterization. The SSPD was operated at liquid helium temperatures inside a cryogenic dip stick. A bias-tee was used to drive a fixed bias current of I = $0.95I_C$ = 15.0 μA through the nanowires. At this bias current, the device shows a dark count rate of <100 cps and an estimated internal detection efficiency of 0.1−1%. A low noise voltage source in series with a 50 kΩ resistor was operated as a constant current source. Voltage pulses arising from single photon detection events were then amplified using two 30 dB high-bandwidth amplifiers and detected with a PicoQuant Timeharp Card 200 time correlated counting module recording histograms of the time intervals between the trigger signal provided by a microwave source and the voltage pulse arising upon photon detection. A continuous wave diode laser source was sent through a Mach−Zehnder electro-optical modulator driven by a 3.3 GHz microwave source. In this way, the laser output was temporally gated into 290 ± 70 ps long Gaussian pulses, as shown in Figure 1c, at a repetition rate of 100 MHz and a duty-cycle of 3%. Using this technique, we temporally filtered the on-chip detected SSPD signal enabling us to separate the scattered laser light from the incoherent part of the QD luminescence signal detected by the SSPD. A detailed description of the complete experimental setup is given in the Supporting Information (section S1). For all off-chip detected confocal PLE measurements the laser was guided through a pulse shaper with a bandwidth of 1 nm suppressing laser sidebands. The light emitted by the QDs was collected with a single mode optical fiber and guided to a 0.5 m focal length spectrometer. Additionally, a 975 nm short/long-pass filter was used in the excitation/detection path. In addition, for the broad PLE sweep presented in Figure 2b, a 980 nm band-pass filter was employed.

■ ASSOCIATED CONTENT

Ⓢ Supporting Information

Description of the experimental setup, detailed PL studies of X_1 and X_3, an analysis of the gating laser power dependence, the SSPD operation parameters, the sample structure, measurements concerning the stray light suppression, and an estimation of the RF count rate on the SSPD. The Supporting Information is available free of charge on the ACS Publications website at DOI: 10.1021/acs.nanolett.5b01444.

■ AUTHOR INFORMATION

Corresponding Authors

*E-mail: finley@wsi.tum.de.
*E-mail: kaniber@wsi.tum.de.

DOI: 10.1021/acs.nanolett.5b01444
Nano Lett. XXXX, XXX, XXX−XXX

Author Contributions

G.R., F.F., M.K., and J.J.F. conceived and designed the experiments. G.R. prepared the samples. G.R. and F.F. performed the experiments and analyzed the data. S.L. assisted with the autocorrelation measurement. A.A., K.M., and R.G. contributed materials. G.R., F.F., M.K., and J.J.F. prepared the manuscript. All authors reviewed the manuscript.

Notes

The authors declare no competing financial interest.

■ ACKNOWLEDGMENTS

We gratefully acknowledge D. Sahin and A. Fiore (TU Eindhoven), K. Berggren and F. Najafi (MIT), and R. Hadfield (University of Glasgow) for useful discussions and the financial support from BMBF via QuaHL-Rep, project number 01BQ1036, Q.com via project number 16KIS0110, the EU via the integrated project SOLID, the DFG via SFB 631-B3, and the ARO (grant W911NF-13-1-0309).

■ REFERENCES

(1) Matthiesen, C.; Vamivakas, A. M.; Atatüre, M. *Phys. Rev. Lett.* **2012**, *108*, 093602.
(2) Laucht, A.; Pütz, S.; Günthner, T.; Hauke, N.; Saive, R.; Frédérick, S.; Bichler, M.; Amann, M.; Holleitner, A.; Kaniber, M.; Finley, J. *Phys. Rev. X* **2012**, *2*, 011014.
(3) Viasnoff-Schwoob, E.; Weisbuch, C.; Benisty, H.; Olivier, S.; Varoutsis, S.; Robert-Philip, I.; Houdré, R.; Smith, C. *Phys. Rev. Lett.* **2005**, *95*, 183901.
(4) Rao, V. S. C.; Hughes, S. *Phys. Rev. Lett.* **2007**, *99*, 193901.
(5) Thyrrestrup, H.; Sapienza, L.; Lodahl, P. *Appl. Phys. Lett.* **2010**, *96*, 231106.
(6) Faraon, A.; Fushman, I.; Englund, D.; Stoltz, N.; Petroff, P.; Vuckovic, J. *Nat. Phys.* **2008**, *4*, 859−863.
(7) Birnbaum, K.; Boca, A.; Miller, R.; Boozer, A.; Northup, T.; Kimble, H. *Nature* **2005**, *436*, 87−90.
(8) Reinhard, A.; Volz, T.; Winger, M.; Badolato, A.; Hennessy, K.; Hu, E.; Imamoglu, A. *Nat. Photonics* **2011**, *6*, 93−96.
(9) Tiarks, D.; Baur, S.; Schneider, K.; Dürr, S.; Rempe, G. *Phys. Rev. Lett.* **2014**, *113*, 053602.
(10) Gorniaczyk, H.; Tresp, C.; Schmidt, J.; Fedder, H.; Hofferberth, S. *Phys. Rev. Lett.* **2014**, *113*, 053601.
(11) Chang, D.; Sørensen, A.; Demler, E.; Lukin, M. *Nat. Phys.* **2007**, *3*, 807−812.
(12) Hwang, J.; Pototschnig, M.; Lettow, R.; Zumofen, G.; Renn, A.; Götzinger, S.; Sandoghdar, V. *Nature* **2009**, *460*, 76−80.
(13) Volz, T.; Reinhard, A.; Winger, M.; Badolato, A.; Hennessy, K.; Hu, E.; Imamoglu, A. *Nat. Photonics* **2012**, *6*, 605−609.
(14) Englund, D.; Faraon, A.; Zhang, B.; Yamamoto, Y.; Vuckovic, J. *Opt. Express* **2007**, *15*, 5550−5558.
(15) Schwagmann, A.; Kalliakos, S.; Farrer, I.; Griffiths, J.; Jones, G.; Ritchie, D.; Shields, A. *Appl. Phys. Lett.* **2011**, *99*, 261108.
(16) Ba Hoang, T.; Beetz, J.; Midolo, L.; Skacel, M.; Lermer, M.; Kamp, M.; Höfling, S.; Balet, L.; Chauvin, N.; Fiore, A. *Appl. Phys. Lett.* **2012**, *100*, 061122.
(17) Pernice, W.; Schuck, C.; Minaeva, O.; Li, M.; Goltsman, G.; Sergienko, A.; Tang, H. *Nat. Commun.* **2012**, *3*, 1325.
(18) Marsili, F.; Bitauld, D.; Fiore, A.; Gaggero, A.; Mattioli, F.; Leoni, R.; Benkahoul, M.; Lévy, F. *Opt. Express* **2008**, *16*, 3191−3196.
(19) Hu, X.; Zhong, T.; White, J.; Dauler, E.; Najafi, F.; Herder, C.; Wong, F.; Berggren, K. *Opt. Lett.* **2009**, *34*, 3607−3609.
(20) Kerman, A.; Dauler, E.; Yang, J.; Rosfjord, K.; Anant, V.; Berggren, K.; Goltsman, G.; Voronov, B. *Appl. Phys. Lett.* **2007**, *90*, 101110.
(21) Reithmaier, G.; Senf, J.; Lichtmannecker, S.; Reichert, T.; Flassig, F.; Voss, A.; Gross, R.; Finley, J. *J. Appl. Phys.* **2013**, *113*, 143507.
(22) Kitaygorsky, J.; Komissarov, I.; Jukna, A.; Pan, D.; Minaeva, O.; Kaurova, N.; Divochiy, A.; Korneev, A.; Tarkhov, M.; Voronov, B.; Milostnaya, I.; Goltsman, G.; Sobolewski, R. *IEEE Trans. Appl. Supercond.* **2007**, *17*, 275−278.
(23) Hofherr, M.; Rall, D.; Ilin, K.; Siegel, M.; Semenov, A.; Hübers, H.; Gippius, N. *J. Appl. Phys.* **2010**, *8*, 014507.
(24) Goltsman, G. N.; Korneev, A.; Rubtsova, I.; Milotsnaya, I.; Chulkova, G.; Minaeva, O.; Smirvov, K.; Voronov, B.; Slysz, W.; Pearlman, A.; Verevkin, A.; Sobolewski, R. *Phys. Status Solidi C* **2005**, *2*, 1480−1488.
(25) Najafi, F.; Marsili, F.; Dauler, E.; Molnar, R.; Berggren, K. *Appl. Phys. Lett.* **2012**, *100*, 152602.
(26) Skocpol, W.; Beasley, M.; Tinkham, M. *J. Appl. Phys.* **1974**, *45*, 4054.
(27) Matthews, J.; Politi, A.; Stefanov, A.; O'Brien, J. *Nat. Photonics* **2009**, *3*, 346−350.
(28) Sprengers, J.; Gaggero, A.; Sahin, D.; Jahanmirinejad, S.; Frucci, G.; Mattioli, F.; Leoni, R.; Beetz, J.; Lermer, M.; Kamp, M.; Höfling, S.; Sanjines, R.; Fiore, A. *Appl. Phys. Lett.* **2011**, *99*, 181110.
(29) Politi, A.; Matthews, J.; Thompson, M.; O'Brien, J. *IEEE J. Sel. Top. Quantum Electron.* **2009**, *15*, 1673−1684.
(30) Heeres, R.; Kouwenhoven, L.; Zwiller, V. *Nat. Nanotechnol.* **2013**, *8*, 719−722.
(31) Heeres, R.; Dorenbos, S.; Koene, B.; Solomon, G.; Kouwenhoven, L.; Zwiller, V. *Nano Lett.* **2010**, *10*, 661−664.
(32) Walther, P.; Resch, K.; Rudolph, T.; Schenck, E.; Weinfurter, H.; Vedral, V.; Aspelmeyer, M.; Zeilinger, A. *Nature* **2005**, *434*, 169−176.
(33) Knill, E.; Laflamme, R.; Milburn, G. *Nature* **2001**, *409*, 46−52.
(34) Reithmaier, G.; Flassig, F.; Hasch, P.; Lichtmannecker, S.; Müller, K.; Vuckovic, J.; Gross, R.; Kaniber, M.; Finley, J. *Appl. Phys. Lett.* **2014**, *105*, 081107.
(35) Reithmaier, G.; Lichtmannecker, S.; Reichert, T.; Hasch, P.; Müller, K.; Bichler, M.; Gross, R.; Finley, J. *Sci. Rep.* **2013**, *3*, 1901.
(36) Finley, J.; Ashmore, A.; Lemaître, A.; Mowbray, D.; Skolnick, M.; Itskevich, I.; Maksym, P.; Hopkinson, M.; Krauss, T. *Phys. Rev. B: Condens. Matter Mater. Phys.* **2001**, *3*, 073307.
(37) Vasanelli, A.; Ferreira, R.; Bastard, G. *Phys. Rev. Lett.* **2002**, *89*, 216804.
(38) Finley, J.; Fry, P.; Ashmore, A.; Lemaître, A.; Tartakovskii, A.; Oulton, R.; Mowbray, D.; Skolnick, M.; Hopkinson, M.; Buckle, P.; Maksym, P. *Phys. Rev. B: Condens. Matter Mater. Phys.* **2001**, *63*, 161305.
(39) Nguyen, H.; Sallen, G.; Voisin, C.; Roussignol, P.; Diederichs, C.; Cassabois, G. *Phys. Rev. Lett.* **2012**, *108*, 057401.
(40) Makhonin, M.; Dixon, J.; Coles, R.; Royall, B.; Clarke, E.; Skolnick, M.; Fox, A. *arXiv 1404.3967*, 2014.
(41) Brouri, R.; Beveratos, A.; Poizat, J.; Grangier, P. *Opt. Lett.* **2000**, *25*, 1294.
(42) Gaggero, A.; Jahanmiri Nejad, S.; Marsili, F.; Mattioli, F.; Leoni, R.; Bitauld, D.; Sahin, D.; Hamhuis, G.; Nötzel, R.; Sanjines, R.; Fiore, A. *Appl. Phys. Lett.* **2010**, *97*, 151108.
(43) Marsili, F.; Gaggero, A.; Li, L.; Surrente, A.; Leoni, R.; Lévy, F.; Fiore, A. *Supercond. Sci. Technol.* **2009**, *22*, 095013.

DOI: 10.1021/acs.nanolett.5b01444
Nano Lett. XXXX, XXX, XXX−XXX